

# Piezoelectric-Effect Enhanced Perovskite Plasmonic Nanolasers

Meili Li, Junfeng Lu, Peng Wan, Mingming Jiang, Feng Lin, Xianxin Wu, Xinfeng Liu, and Caofeng Pan\*

Herein, the piezoelectric effect of CsPbBr<sub>3</sub> perovskite is utilized for the first time to enhance the nanolasers performance based on the flexible poly(ethylenenaphthalate) PEN/single-crystal-Au/MgF<sub>2</sub>/CsPbBr<sub>3</sub> (ScAu/M/CPB) structure. The dynamic-modulated plasmonic lasing mode blueshift is achieved by the piezoelectric polarization effect (PPE)-induced effective refractive index ( $n_{\text{eff}}$ ) change by varying the applied strain ( $\epsilon$ ). In particular, taking advantage of the increased cavity mode frequency, the lasing threshold ( $P_{\text{th}}$ ) reduces from 4.5  $\mu\text{J cm}^{-2}$  ( $\epsilon = 0$ ) to 1.5  $\mu\text{J cm}^{-2}$  ( $\epsilon = -1.02\%$ ). The  $\epsilon$ -dependent carrier dynamics results reveal the nature of ultralow  $P_{\text{th}}$  being PPE-induced spontaneous emission (SE) decay rate enhancement, leading to the reduction in radiation loss of the plasmonic cavity. The corresponding enhancement mechanism is put forward to elucidate the principle of piezoelectric-induced dynamic modulation nanolasers characteristic. This work demonstrates that coupling of piezoelectric effect and plasmonics is an effective route to enhance the performance of plasmonic nanolasers.

propagating SP along the planar metallic surface, so-called SP polariton (SPP) it can lower the plasmonic cavity loss by suppressing the radiation loss.<sup>[4,5]</sup> However, it inevitably introduces the nonradiative decay channel of free carrier absorption in metal which can be dominant over the radiation loss and the gain material loss.<sup>[5-7]</sup> More efforts to improve metal quality have included the introduction of high-quality sodium films<sup>[8]</sup> and single-crystalline silver (Ag)<sup>[9]</sup> or aluminum (Al) films,<sup>[10]</sup> which have been successfully reduced the threshold of nanolasers. Meanwhile, metal trihalide perovskites (ABX<sub>3</sub>, A: Cs<sup>+</sup>, MA<sup>+</sup>, FA<sup>+</sup>, B: Pb<sup>2+</sup>) exhibit strong light-matter interaction, which have been realized ultrahigh Purcell enhancement of 209 in a subwavelength lasing cavity.<sup>[3,9,11-13]</sup> Nevertheless, to further lower the threshold, optimization of

## 1. Introduction

Surface plasmon (SP) is an electromagnetic mode of photons and electrons at the interface between dielectric and metal, which provides a novel means of enhancing light-matter interaction at nanoscale.<sup>[1-3]</sup> The energy-momentum dispersion of

the cavity configuration, and mitigating the radiation loss are still necessary.

The strain-induced piezophototronic effect has played important roles for regulating the performance of photodectors,<sup>[14,15]</sup> solar cells,<sup>[16,17,18]</sup> light-emitting diodes (LEDs),<sup>[19,20]</sup> and electrically pumped lasing.<sup>[21]</sup> The major principle of piezophototronic effects is using strain-generated piezoelectric polarization charges at the interface to modulate carrier dynamic processes.<sup>[18,22]</sup> As for ABX<sub>3</sub>, such effects stem from the breaking of crystal centrosymmetry.<sup>[16,23-25]</sup> When properly strain applied along the growth direction of ABX<sub>3</sub> perovskite, the dipole center of the cation and anion separate, leading to the electric dipole moments which will create a piezoelectric potential within the crystal, namely, PPE.<sup>[16,23,26]</sup> PPE can modulate the lasing mode of semiconductor materials due to the piezoelectric polarization-induced refractive index change, such as CsPbBr<sub>3</sub>,<sup>[26]</sup> ZnO,<sup>[27-29]</sup> CdS,<sup>[30]</sup> and GaN materials.<sup>[31]</sup> Moreover, perovskite materials are highly susceptible to light,<sup>[32]</sup> temperature,<sup>[33]</sup> pump energy,<sup>[34]</sup> and pressure,<sup>[35]</sup> which indicates a great tunability of the optical devices. Hence, these results offer a new strategy for dynamically modulating the characteristics of the plasmonic nanolasers.


Herein, we designed the poly(ethylenenaphthalate) PEN/single-crystal-Au/MgF<sub>2</sub>/CsPbBr<sub>3</sub> (ScAu/M/CPB) flexible plasmon devices, where compressive strain further can be exerted on the CsPbBr<sub>3</sub> nanobelt (CPNB) via applying bending stress to the PEN substrate. Utilizing the optical excitation and PPE of CPB for the first time, we demonstrated that the lasing

M. Li, C. Pan  
 Beijing Institute of Nanoenergy and Nanosystems  
 Chinese Academy of Sciences  
 Beijing 100400, P. R. China  
 E-mail: cfpan@binn.cas.cn

J. Lu, P. Wan, M. Jiang  
 Department of Applied Physics  
 College of Science  
 Nanjing University of Aeronautics and Astronautics  
 Nanjing 211106, P. R. China

F. Lin  
 Institute of Condensed Matter and Material Physics  
 Peking University  
 Beijing 100871, P. R. China

X. Wu, X. Liu  
 CAS Key Laboratory of Standardization and Measurement for Nanotechnology  
 CAS Center of Excellence for Nanoscience  
 National Center for Nanoscience and Technology  
 Beijing 100190, P. R. China

 The ORCID identification number(s) for the author(s) of this article can be found under <https://doi.org/10.1002/adom.202202723>.

DOI: 10.1002/adom.202202723

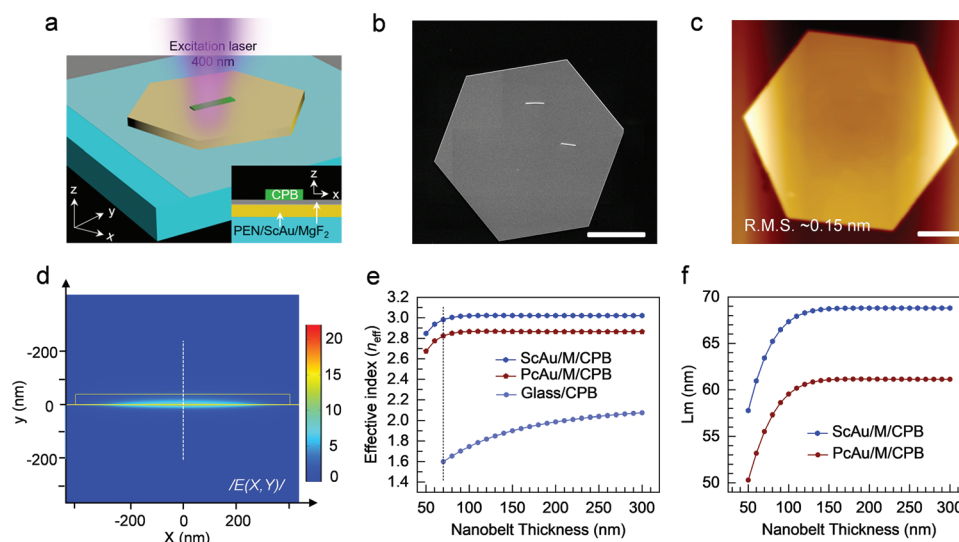


**Figure 1.** Room temperature plasmonic nanolaser device. a) Schematic of ScAu/M/CPB plasmonic device: a CPBNB is supported on ScAu microflakes with 5-nm MgF<sub>2</sub> insulator separation layer. A focused femtosecond pulsed laser (400 nm, 100 fs) source is used to pump the whole CPBNBs. The CsPbBr<sub>3</sub> photonluminescence waveguides along the high refractive nanobelt, hybridize with SPP mode of ScAu microflake to produce plasmonic lasing. b) SEM image of the CPBNBs sitting on MgF<sub>2</sub>/ScAu microflake. The NB length is ≈9 μm and the scale bar is 20 μm. c) AFM image of the ScAu microflake with a root-mean-square roughness of ≈0.15 nm. d) Absolute electric field ( $|E|$ ) distribution around the plasmonic device with a wavelength of  $\lambda = 540$  nm, corresponds to the lasing wavelength of CPBNBs, calculated by a finite element method. e) The effective index of the photonic (glass/CsPbBr<sub>3</sub>) and hybrid plasmonic mode (ScAu/M/CPB and PcAu/M/CPB) as a function of NB thickness with the incident wavelength at 540 nm. f) The ScAu/M/CPB modes (blue solid dots) propagation distance compared with PcAu/M/CPB modes (deep red solid dots) with the incident wavelength at 540 nm.

threshold ( $P_{th}$ ) has been dynamically reduced effectively from  $4.5 \mu\text{J cm}^{-2}$  to  $1.5 \mu\text{J cm}^{-2}$  under compressive strain ( $\varepsilon = 0$  to  $-1.02\%$ ), with a ≈66% enhancement. The time-resolved photoluminescence (TRPL) analyses suggest the spontaneous emission (SE) decay rate of ScAu/M/CPB device is enhanced ≈50% compared with without strain, and the Purcell factors increased from 6.8 to 12.5, which certifies the increased energy-exchange rate between the exciton and SPP mode. A corresponding mechanism was proposed to elucidate the principle to boost the performance of ScAu/M/CPB nanolasers. Our work not only present a new strategy to improve the performance of plasmonic nanolasers, but also will further extend the application in flexible laser and on-chip strain sensing.

## 2. Results And Discussion

Figure 1a schematically illustrates the device construction and Figure 1b is a scanning electron microscope (SEM) image. The device (ScAu/M/CPB) consists of a rectangular CPBNB sitting on the ScAu microflake separated with a thin insulating gap layer (≈5 nm) of magnesium fluoride (MgF<sub>2</sub>) (Note S1, Supporting Information). Monocrystalline Au microflakes are adopted as the plasmonic medium by reason of its atomically smooth surface and high crystallinity, the roughness of continuous ScAu/MgF<sub>2</sub> film is only 0.3 nm which can reduce the metal scattering loss (Figure 1c, Figures S1 and S2, Supporting Information).<sup>[8–10,36]</sup> Moreover, high-quality CPBNBs exhibit planar cross sections with the thickness of  $\approx 76 \pm 1$  nm and a width of  $\approx 1 \pm 0.2 \mu\text{m}$  (Figure S3, Supporting Information), which can construct an entire-contact planar interface to suppress the edge and interface scattering loss.<sup>[36]</sup> Evidence of

the high-quality single-crystal CPBNBs is provided in the Supporting Information (Figures S3 and S4, Supporting Information). The SP effect strongly confine the electromagnetic field at the interface between ScAu and CPBNB (Figure 1d and Figure S5, Supporting Information).<sup>[3,11,36]</sup> Moreover, compared with PEN/polycrystalline-Au/MgF<sub>2</sub>/CsPbBr<sub>3</sub> (PcAu/M/CPB) device, ScAu/M/CPB devices are of the larger  $n_{eff}$  and lower propagation loss ( $L_m$ ), representing the stronger optical mode confinement (Figure 1e and Figure 1f, Figure S6, Supporting Information).<sup>[3,8,11,13]</sup> Therefore, ScAu/M/CPB devices were selected in our experiments with the lower  $P_{th}$  ( $\approx 4.0 \pm 0.5 \mu\text{J cm}^{-2}$ ), which can compare with photonic laser devices ( $\approx 4.2 \pm 0.3 \mu\text{J cm}^{-2}$ ) and far below PcAu/M/CPB ( $\approx 10 \pm 1 \mu\text{J cm}^{-2}$ ) devices (Table S1 and Figure S7, Supporting Information).

The power ( $P$ )-dependent emission spectra of a ScAu/M/CPB device (CPBNB: length  $L \approx 8.0 \mu\text{m}$ , width  $W \approx 1.0 \mu\text{m}$ , and thickness  $T \approx 76$  nm; Figure S3, Supporting Information) under femtosecond pulsed laser (400 nm, 100 fs) is shown in Figure 2a. At  $P$  ( $P \approx 1.07 - 3.88 \mu\text{J cm}^{-2}$ ) less than  $P_{th}$ , we observed a broad SE band centered at 530 nm with a full width at half-maximum (FWHM) of ≈15 nm. At  $P > P_{th}$  ( $P > 3.88 \mu\text{J cm}^{-2}$ ), a dominant lasing mode become at 535.4 nm with a much narrower linewidth ( $\delta\lambda \approx 0.268$  nm) than SE, which is the SP mode selectively amplified by strong confinement in the device and suggests the occurrence of lasing action.<sup>[11,26,36]</sup> The corresponding  $\mu$ -PL image is shown inset of Figure 2a, exhibiting the stronger emission and light coherence at the two end facets of CPBNB.<sup>[11]</sup> The  $P_{th}$  of this ScAu/M/CPB device can be evidenced by the “S” shaped light-light ( $L - L$ ) curve, which can be extracted from the integrated emission intensity as a function of  $P$  (Figure 2b). The  $L - L$  curve in Figure 2b can be fitted by a classic rate equation model (Note S2, Supporting Information)

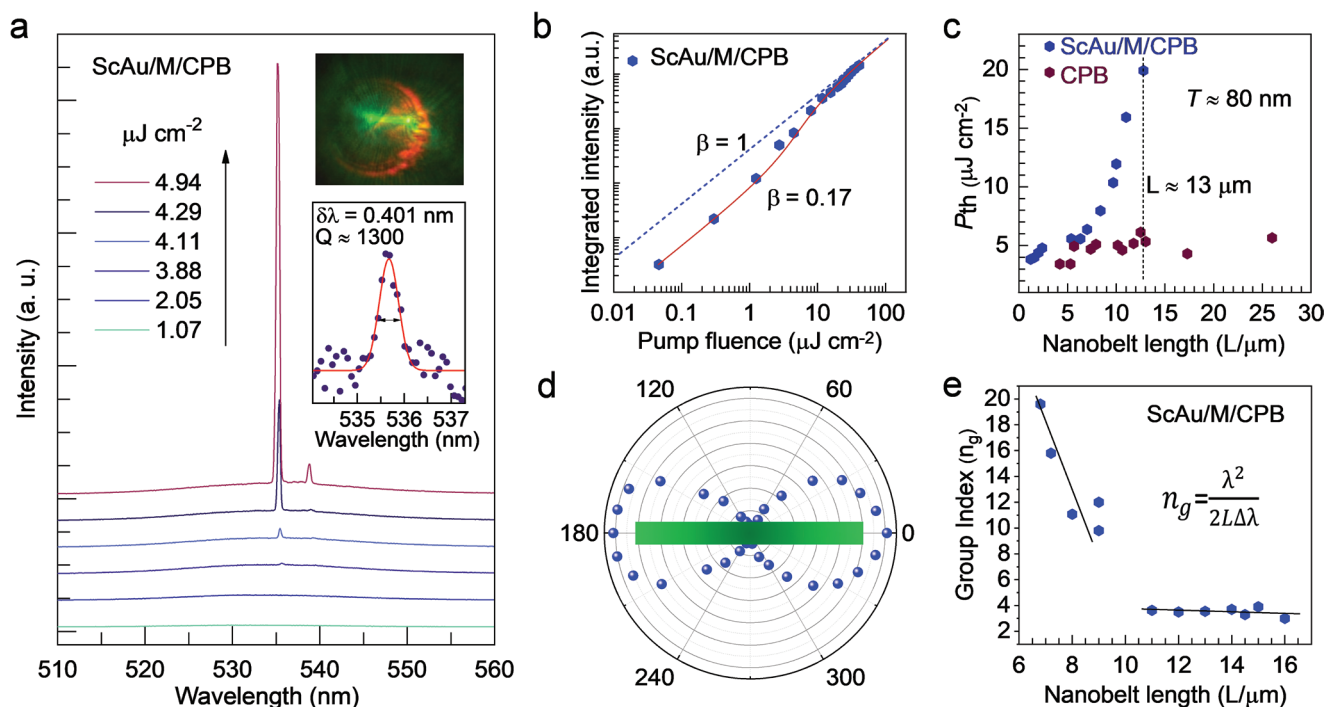


**Figure 2.** Room-temperature ScAu/M/CPB plasmonic lasing characterization. a) Pump-dependent emission spectra of the ScAu/M/CPB plasmonic device with increasing  $P$  from  $1.07 \mu\text{J cm}^{-2}$  (bottom) to  $4.94 \mu\text{J cm}^{-2}$  (top). The nanobelt length is  $\approx 9 \mu\text{m}$ . Inset: optical images at  $P > P_{\text{th}}$  (upper panel) and magnified view of a lasing threshold mode fitted by the Lorentzian function (lower panel). b) Integrated emission intensity as a function of pump power for the 537 nm mode. The blue hexagons represent experimental data and the red solid line represents the fitted result with a SE coupling factor  $\beta = 0.17$  using a simple rate equation. The blue dashed line indicates the ideal nonthreshold lasing behavior with SE coupling factor of 1. c) Threshold intensity of ScAu/M/CPB hybrid plasmonic lasing and photonic lasing versus CPBNBs length ( $L$ ). The thickness ( $T$ ) of these CPBNBs are  $\approx 80 \text{ nm}$ . d) Hybrid plasmonic mode polarization distribution along the CPBNB (the green rectangle,  $T \approx 80 \text{ nm}$ ) sitting on  $\text{MgF}_2/\text{ScAu}$  microflake. e) The group index as the function of CPBNBs is estimated from the mode spacing in lasing emission spectra.

to achieve SE coupling factor  $\beta = 0.17$ , which indicates that about 17% of the total SE is coupled to the cavity mode.<sup>[9,11]</sup> However, the blue dashed assisted line indicates the 100% coupling SE situation, suggesting the nonthreshold plasmonic laser output with  $\beta = 1$ .<sup>[11]</sup> Clear threshold behavior was observed in the  $L - L$  curve ( $P_{\text{th}} \approx 4.0 \pm 0.1 \mu\text{J cm}^{-2}$ ), which, is comparable with the glass/Au grating/MAPbBr<sub>3</sub> nanolaser array structure but significantly lower than that of the as-fabricated polycrystalline-metal-based film plasmonic nanolasers (Table S2, Supporting Information).<sup>[9,11,34,37–43]</sup> The lower lasing threshold usually relies on the high quality-factor ( $Q$ -factor) cavity mode.<sup>[3,11,36]</sup> Specifically, the  $Q$ -factor can be calculated by dividing the mode wavelength (535.6 nm) by the mode linewidth ( $\delta\lambda \approx 0.401 \text{ nm}$ ) near the lasing threshold ( $P = 3.88 \mu\text{J cm}^{-2}$ ,  $Q \approx 1300$ , Figure 2a inset). To our knowledge, this is the highest value among metal halide perovskite-based plasmonic nanolasers (Table S2, Supporting Information).<sup>[9,11,34,37–43]</sup>

As shown in Figure 2c, the  $P_{\text{th}}$  of the ScAu/M/CPB devices significantly increased from  $5.5 \mu\text{J cm}^{-2}$  to  $20 \mu\text{J cm}^{-2}$  when the length of CPBNBs were over  $9.0 \mu\text{m}$ , which suggested the longer plasmonic waveguide and more SPP propagates loss occurring to the plasmonic energy.<sup>[3,11,38]</sup> By contrast, the  $P_{\text{th}}$  of that photonic lasers continued to maintain  $\approx 4.5 \mu\text{J cm}^{-2}$  with varying the length of CPBNBs from 4.2 to 26  $\mu\text{m}$ , which was also demonstrated in previous works.<sup>[11]</sup> In consequence, the total loss of plasmonic laser primarily originates from high

ohmic losses and scattering losses of plasmonic metals, as well as radiative loss of cavity.<sup>[1–3,11,36]</sup> Obviously, the optical loss of CPB gain and the plasmonic metal materials have been optimized to obtain a lower threshold in our work and previous works (Tables S1 and S2, Supporting Information).<sup>[9,11–13,34,37–43]</sup> To further lower the threshold, we utilized the piezoelectric effect of CPB to regulate the electron concentration ( $N_e$ ) on the surface of ScAu via strain-engineering to increase the energy coupling efficiency of the cavity mode.<sup>[44]</sup>

Before applying strain on the ScAu/M/CPB plasmonic devices, we further confirmed the polarization of plasmonic lasing influenced by incidence polarization utilizing the  $\mu$ -PL system. Figure 2d presents the polarization-dependent lasing intensity data of the ScAu/M/CPB device. It can be seen that the lasing intensity of the ScAu/M/CPB device showed a maximum when the polarization was along the  $0^\circ$  axis, which is consistent with the optical simulation results (Figure S8, Supporting Information). As the incident polarization along CPBNB long axis ( $E_{\text{in}}//C$ ), a dominant lasing mode centered at 536 nm exhibited a much higher intensity ( $E_{\text{out}}//C$ ) than the perpendicular direction ( $E_{\text{out}}\perp C$ ), which indicated the electric field (EF) normal to ScAu surface, exhibiting the strongest coupling to SPP (Figure S8, Supporting Information).<sup>[11,36]</sup> These results unambiguously indicate the achievement of plasmonic lasing in ScAu/M/CPB devices. In addition, we proved the photonic to plasmonic modes jumping by tracking the group index ( $n_g$ )

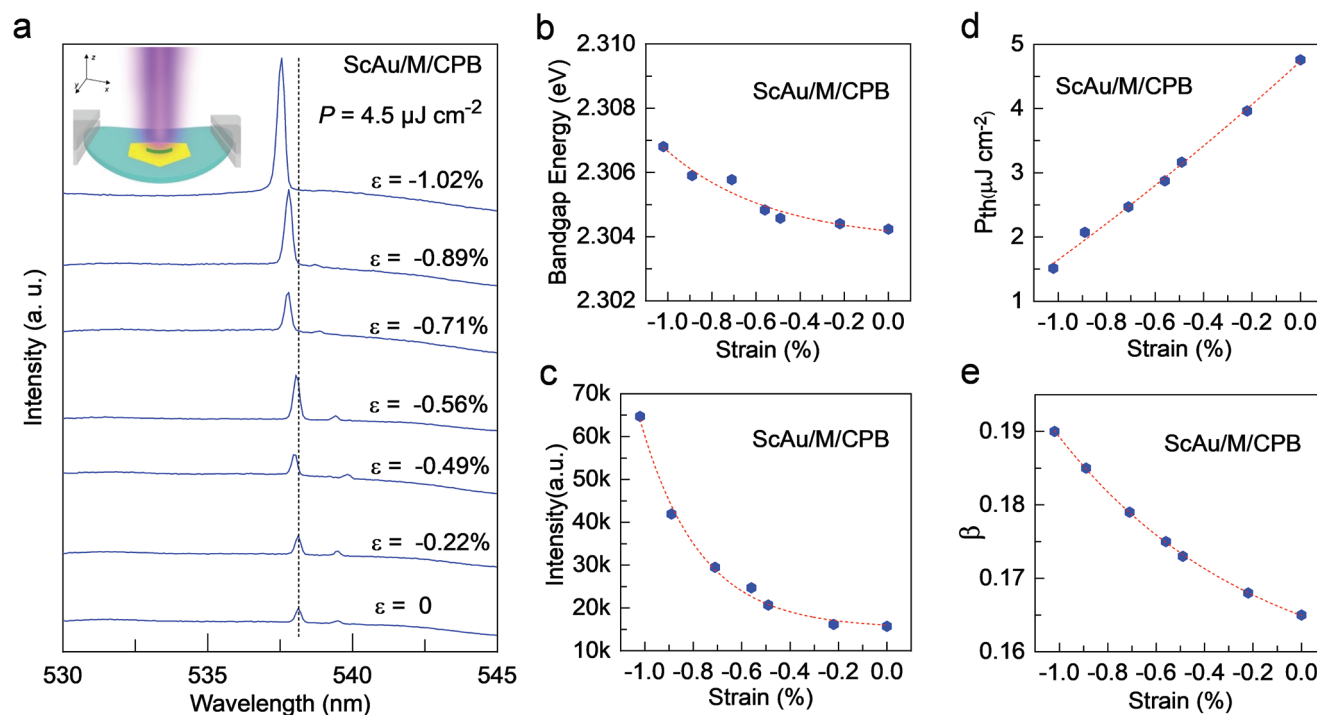


**Figure 3.** Lasing characteristics dynamic regulation under compressive strain for ScAu/M/CPB plasmonic device. a) Spectra of stimulated emission for ScAu/M/CPB device under different degrees of compressive strain from  $\varepsilon = 0\%$  to  $\varepsilon = -1.02\%$  as  $P = 4.5 \mu\text{J cm}^{-2}$ . Illustration is schematic of ScAu/M/CPB plasmonic device under compressive state using femtosecond pulsed laser pump (400 nm, 100 fs). Variation of the b) lasing mode photon energy, c) lasing emission intensity, d) lasing threshold, and e) SE coupling factor  $\beta$  values as a function of the compressive strain.

of the SP lasing modes.<sup>[3,8,45]</sup> To be specific, the higher  $n_g$  of the SP modes usually results in stronger boundary reflection compensating for the optical absorption loss in metals, according to  $n_g = \frac{\lambda^2}{2L\Delta\lambda}$ , where  $\lambda$  is the resonance wavelength,  $\Delta\lambda$  is mode spacing.<sup>[3,8,11]</sup> As shown in Figure 2e, a sudden clearly increase of the  $n_g$  from 3.63 to 12 when the length of CPBNBs were below  $9 \mu\text{m}$ , which indicated the dominant plasmonic mode in smaller cavities as well as the enhanced boundary reflection (Figure S9 and Table S3, Supporting Information).<sup>[3,8]</sup> Therefore, we selected the critical length of CPBNBs ( $\approx 8.0\text{--}9.0 \mu\text{m}$ ,  $n_g \approx 11.2$ ,  $P_{th} \approx 5.0 \mu\text{J cm}^{-2}$ ) from photonic to plasmonic modes jumping as a model microcavity to analyze the piezoelectric effect on the ScAu/M/CPB devices.

We further conducted the compressive strain-dependent lasing spectra measurement. The compressive strain was applied on the ScAu/M/CPB device (CPBNB length  $\approx 9 \mu\text{m}$ ) by bending the flexible PEN substrate via 3D manual stages (Figure 3a inset, Method in Note S1, Supporting Information).<sup>[26–31]</sup> As  $P = 4.5 \mu\text{J cm}^{-2}$ ,  $\varepsilon = 0\%$ , two distinct lasing modes emerged at the low-energy side of the SE peak (Figure 3a, Figure S10, Supporting Information). As applied  $\varepsilon$  increases from  $0\%$  to  $-1.02\%$ , the lasing mode of the high-energy side occurred blueshift from 538 to 537.5 nm. It can be seen that the photon energy increased  $\approx 3 \text{ meV}$  (Figure 3b), which suggested the photon frequency of CPBNB increasing. When the  $\varepsilon$  reached  $-0.71\%$ , just a single-mode lasing emerged couple with disappearance of the low-energy side mode. Moreover, we further carried out  $\varepsilon$ -mediate lasing measurement on PcAu/M/CPB device

and photonic device, the lasing mode both exhibited blueshift (Figures S11 and S12, Supporting Information). Therefore, the strain-engineering can also dynamically modulate the lasing modes of plasmonic nanolaser. Nevertheless, the mechanisms leading to the movement of the plasmonic mode is attributed to altering of  $n_{eff}$  (from  $\approx 2.92$  decreasing to  $\approx 2.76$ ), which is caused by the increased  $N_e$  on the ScAu surface due to PPE of CPB (Figures S13 and S14, Note S3, Supporting Information).<sup>[26–31,44]</sup> This result pellucid explain the underlying mechanism of plasmonic spectral blueshift.

Figure 3a also clearly shows the lasing intensity gradually increased with increasing of the  $\varepsilon$  from  $0\%$  to  $-1.02\%$ , with an enhancement of  $\approx 70\%$  (Figure 3c). We assume that such strain-induced emission enhancement may be ascribed to: 1) the direct semiconducting characteristics enhancement,<sup>[46]</sup> 2) the lattice contraction leading to decreased the defect density,<sup>[47–49]</sup> or 3) piezoelectric effect, and their effects are listed in Note S4 (Supporting Information). The band structure of CPB was calculated by utilizing the density functional theory (DFT) under  $\varepsilon$  from  $0\%$  to  $-1.02\%$ . It can be seen that the bulk CPB is a direct bandgap semiconductor with the band gap located at 2.296 eV, but the direct semiconducting characteristics were not reinforced under different  $\varepsilon$  (Figure S15, Supporting Information).<sup>[50]</sup> Although the lattice contraction will decrease the defect density of semiconductor materials, however, this effect is not evident in bulk materials.<sup>[26,49]</sup> We did not find an obvious increase or degradation in the PL and laser intensity based on photonic device PEN/CPB (Figures S12 and S16, Supporting Information).<sup>[26]</sup> Nevertheless, the output lasing

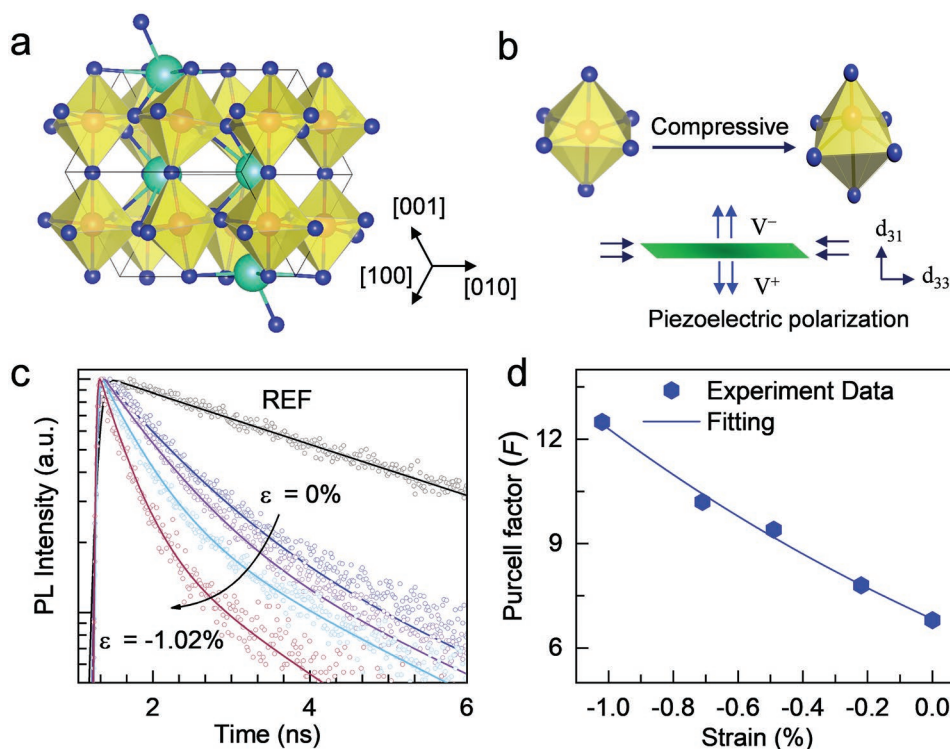


**Figure 4.** Mechanism analysis of the piezoelectric effect and strain-dependent carrier dynamics of CPBNB. a) Schematic illustration of the CPB perovskite structure with the  $\text{PbBr}_6$  octahedral network. b) Schematic diagrams showing the individual octahedra structure from the normal state to the compressive state (upper panel), and the generation of a piezopotential along the [001] direction of the CPBNB (the green rectangle) under applying compressive strain along the [010] direction due to the piezoelectric polarization effect of CPB (lower panel).  $V^+$  and  $V^-$  represent the piezopotential.  $d_{33}$  and  $d_{31}$  are the transverse and longitudinal piezoelectric coefficients, respectively. c) TRPL decay curves of CPBNB on  $\text{MgF}_2/\text{ScAu}/\text{PEN}$  substrate with applying compressive strain from  $\epsilon = 0\%$  (blue dots) to  $\epsilon = -1.02\%$  (red dots). d) Plot of the Purcell factor estimated from emission lifetime  $\tau$  as a function of compressive strain for  $\text{ScAu}/\text{M}/\text{CPB}$  device. The blue hexagons are the experimental data and the solid line is a fit to the data.

intensity increased  $\approx 50\%$  based on  $\text{PcAu}/\text{M}/\text{CPB}$  devices when applied the  $\epsilon$  from  $0\%$  to  $-1.31\%$  (Figure S11, Supporting Information). Therefore, these results well indicate that the piezoelectric effect-induced the increasing of  $N_e$  on  $\text{ScAu}$  surface has a key role in the enhancement of lasing intensity for plasmonic nanolasers.<sup>[44]</sup>

Similarly, the  $P_{\text{th}}$  of the  $\text{ScAu}/\text{M}/\text{CPB}$  devices shown a monotonic reducing from  $\approx 4.5 \mu\text{J cm}^{-2}$  to  $\approx 1.5 \mu\text{J cm}^{-2}$  with increasing of the  $\epsilon$  from  $0\%$  to  $\approx 1.02\%$ , with the performance of 66% enhancement (Figure 3d). A comparison of our results for  $\text{ScAu}/\text{M}/\text{CPB}$  device with previously reported on perovskite plasmonic lasers are summarized in Table S2 (Supporting Information), which is the lowest values reported in the literature.<sup>[9,11–13,34,37–43]</sup> In addition, a similar phenomenon is observed in  $\text{PcAu}/\text{M}/\text{CPB}$  device (Figure S11, Supporting Information), but the strain has no influence on  $P_{\text{th}}$  for the photonic device (Figure S12, Supporting Information).<sup>[26]</sup> More importantly, we found that the  $\beta$ -factor increases from  $\approx 0.166$  to  $\approx 0.19$  as enhancement of the  $\epsilon$  from  $0\%$  to  $-1.02\%$  for  $\text{ScAu}/\text{M}/\text{CPB}$  device (Figure 3e, Figure S17, Supporting Information), which is in accordance with the enhancement of energy-coupling strength between the exciton and SPP mode due to the increased  $N_e$  on the  $\text{ScAu}$  surface.<sup>[11,36,44]</sup> Thus, we attribute these results to the piezoelectric effect, which plays a key role in strain-induced the enhancement of lasing characteristics for plasmonic nanolaser.

How to validate the piezoelectric effect in plasmonic device is an important issue. CPB is an  $\text{ABX}_3$ -type semiconductor, which consists of corner-sharing  $[\text{PbBr}_6]^{4-}$  octahedron and Cs cations confined within the dodecahedral.<sup>[24–26,51]</sup> Figure 4a illustrates the CPB structure using Visualization for Electronic and Structure Analysis (VEST) software. According to the X-ray diffraction (XRD) pattern analysis that the CPB crystal structure is orthorhombic (Figure S3, Supporting Information), which is an asymmetrical structure.<sup>[26,45,51]</sup> When apply compressive strain along the [010] growth direction of the CPBNB, individual octahedra framework will become more distorted, while the central Pb atoms in the octahedra are displaced further away from their original positions along with the lattice expansion in the vertical plane (Figure 4b up panel).<sup>[24–26]</sup> Namely, the  $[\text{PbBr}_6]^{4-}$  octahedral framework is straightened in the vertical direction by compressive strain, where elongated the lattice is along the [001] direction but contracted it in the [010] and [100] plane.<sup>[24,25]</sup> Clearly, the piezoelectric potential is stronger in [001] direction than [010] and [100] direction in CPBNB due to the larger lattice expanded and polarization intensity along the [001] direction under compressive strain.<sup>[24–25]</sup> Thus, the piezoelectric polarization charge will exist mostly in the [001] direction of CPBNB with applied compressive strain due to the PPE (Figure 4b down panel, black arrows represent the direction of applied strain and blue arrows represent the direction of polarization).<sup>[24,26,52]</sup> Since the polarization direction is perpendicular

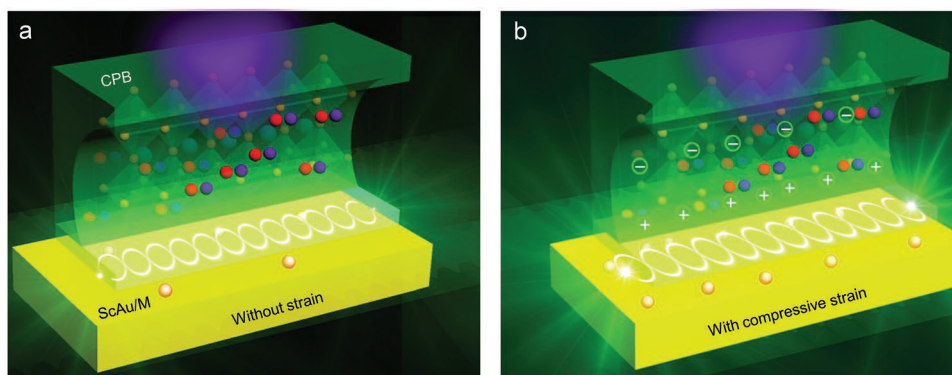


**Figure 5.** Schematic illustrations of the ScAu/M/CPB plasmonic device demonstrating the piezophototronic effect. Schematic drawing describing the exciton (red and purple ball) coupling with electron (pale pink ball) to form SPP in the ScAu/M/CPB device under a 400 nm femtosecond optical excitation: a) without applying strain, b) after applying compressive strain,  $N_e$  increased on the Au surface due to electrostatic interaction. The positive and negative signs represent piezoelectric polarization charges, respectively.

to the applied strain direction, so the piezoelectric potential in CPBNB can be attributed to the combined contribution from the piezoelectric coefficient  $d_{33}$  and  $d_{31}$ , but the  $d_{31}$  in the direction of [001] plays a dominant role.<sup>[23,52,53]</sup> We further calculated the piezopotential distribution in the CPBNB via finite element method (Figure S18, Supporting Information). When the PEN substrate was bent down, the upper surface of CPBNBs will generate compressive strain (Figure 3a inset). Therefore, the face of CPBNB in contact with ScAu was stretched which will generate the positive piezoelectric charges, giving rise to increase interfacial  $N_e$  due to the electrostatic interaction.<sup>[18,22,44]</sup>

TRPL spectrum was further utilized to explore the effect of piezoelectric effect on photo-generated carrier dynamic in ScAu/M/CPB device. Figure 4c shown the emission performance modified by plasmon under low  $P$  ( $P \approx 4 \mu\text{J cm}^{-2}$ ) with applied  $\varepsilon$  from 0% to  $-1.02\%$ . A larger CPBNB photonic device on glass substrate served as the reference sample (Figure S19, Supporting Information), which is defined as the free-space lifetime of CPB and the fitted emission lifetime is  $\tau_{\text{ref}} \approx 5 \pm 0.09$  ns (Figure 4c black circle, donated as REF).<sup>[11,36]</sup> Compared with CPB photonic device, the SE decay rate of ScAu/M/CPB device is remarkably enhanced own to Purcell effect, thus the exciton decay lifetime  $\tau$  is down to  $\approx 0.74 \pm 0.05$  ns (Figure 4c blue circle).<sup>[3,11,36]</sup> When applied  $\varepsilon$  on ScAu/M/CPB device from 0% to  $-1.02\%$ , the radiative recombination lifetime of exciton can be reduced from  $\tau \approx 0.74 \pm 0.05$  ns to  $\tau \approx 0.4 \pm 0.03$  ns (Figure 4c red circle). Therefore, the compressive-strain-induced strong SE decay rate modifies its emissive behavior, leading to the increased Purcell factor from 6.8 to 12.5 as  $\varepsilon$  increased from 0% to  $-1.02\%$  (Figure 4d).<sup>[11,36]</sup> This clearly reveals the compressive strain enhanced energy-exchange rate between exciton and SPP in the plasmonic device.<sup>[11,36]</sup> Thus, the underlying mechanism of strain-induced enhancement of lasing characteristics in plasmonic device is the increased of  $N_e$  on ScAu surface due to the PPE of CPB.

A representative model is proposed to explain the mechanism of piezoelectric effect-enhanced plasmonic nanolaser under compressive strain. The schematic structure of ScAu/M/CPB device after excitation is demonstrated in Figure 5a. After applying compressive strain on CPBNB, the positive piezoelectric charges were generated at the interface between CPBNB and ScAu due to the PPE (Figure 5b).<sup>[18,22,26,44]</sup> The positive piezoelectric

charges at the interface induced more electrons (pale pink balls) on the ScAu surface due to electrostatic interactions, resulting in the lasing mode blueshift and increasing the frequency of cavity mode. Therefore, the coupling efficiency between the excitons and SPP was improved since the frequency of cavity mode ( $5.58 \times 10^{14}$  Hz) is closer to the plasmon resonance frequency of Au ( $7.14 \times 10^{14}$  Hz), which is beneficial to enhance the radiative recombination.<sup>[36,54]</sup> Therefore, the excitons first recombine non-radiative and effectively transfer their energy to the metal system to form the plasmons.<sup>[13,36]</sup> Subsequently, more and more SPs are therefore created via the SP stimulating the excitons in CPB under compressive strain, realizing a high efficiency of non-radiative energy-transfer between exciton and SP.<sup>[36]</sup> Correspondingly, the CPBNB laser on the ScAu/M/CPB structure exhibits  $\approx 66\%$  reduction in the  $P_{\text{th}}$ , primarily due to the coupling of the piezoelectric effect and plasmonic.

### 3. Conclusion

In summary, the performance of the flexible ScAu/M/CPB nanolasers were effectively enhanced by the piezoelectric effect. The threshold was reduced by nearly 66% under compressive strain ( $\varepsilon = -1.02\%$ ). The dynamic modulation of the threshold can be attributed to the positive piezoelectric potential between the interface of the ScAu and CPBNB, more electrons accumulate at the ScAu surface. The role of increasing  $N_e$  on this interface: 1) the  $n_{\text{eff}}$  of the plasmonic composite cavity reduced which caused the lasing mode blueshift. 2) causing an increase in the plasmon resonant frequency, improving the coupling efficiency between excitons and SPP, thus reducing the radiative loss. Our work may provide a novel approach to enhance the lasing performance of piezoelectric semiconductor materials and will extend the application for the piezoelectric effect in flexible laser and on-chip strain sensing and so on.

### Supporting Information

Supporting Information is available from the Wiley Online Library or from the author.

## Acknowledgements

The authors acknowledge the funding support from the National Natural Science Foundation of China (Nos. 62105035, U20A20166, 52125205, and 52192614), National key R&D program of China (Nos. 2021YFB3200302 and 2021YFB3200304), Natural Science Foundation of Beijing Municipality (Nos. Z180011 and 2222088), Shenzhen Science and Technology Program (No. KQTD20170810105439418) and the Fundamental Research Funds for the Central Universities.

## Conflict of Interest

The authors declare no conflict of interest.

## Author Contributions

P.C. conceived the idea. M.L. designed the experiments and wrote the manuscript. M.L. prepared the samples and performed all the spectroscopy measurements.

## Data Availability Statement

The data that support the findings of this study are available from the corresponding author upon reasonable request.

## Keywords

CsPbBr<sub>3</sub> nanobelt, piezoelectric effect, plasmonic nanolasers, single-crystal Au, ultra-low threshold

Received: November 15, 2022

Revised: December 21, 2022

Published online:

- [1] Y. Liang, C. Li, Y.-Z. Huang, Q. Zhang, *ACS Nano* **2020**, *14*, 14375.
- [2] R. Ma, R. Oulton, *Nat. Nanotechnol.* **2019**, *14*, 12.
- [3] S. Cho, Y. Yang, M. Soljačić, S. Yun, *Sci. Adv.* **2021**, *7*, eabf3362.
- [4] C. Li, Z. Liu, Q. Shang, Q. Zhang, *Adv. Opt. Mater.* **2019**, *7*, 1900279.
- [5] S. Wang, H. Chen, R. Ma, *Nano Lett.* **2018**, *18*, 7942.
- [6] S.-L. Wang, S. Wang, X. Man, R. Ma, *Nanophotonics* **2020**, *9*, 3403.
- [7] R. Ma, *Nat. Mater.* **2019**, *18*, 1146.
- [8] Y. Wang, J. Yu, Y. Mao, J. Chen, S. Wang, H. Chen, Y. Zhang, S. Wang, X. Chen, T. Li, L. Zhou, R. Ma, S. Zhu, W. Cai, J. Zhu, *Nature* **2020**, *581*, 401.
- [9] J. Wang, X. Jia, Z. Wang, W. Liu, X. Zhu, Z. Huang, H. Yu, Q. Yang, Y. Sun, Z. Wang, S. Qu, J. Lin, P. Jin, Z. Wang, *Nanoscale* **2020**, *12*, 16403.
- [10] Y. Chou, Y.-M. Wu, K.-B. Hong, B.-T. Chou, J.-H. Shih, Y. Chung, P. Chen, T.-R. Lin, C.-C. Lin, S. Lin, T.-C. Lu, *Nano Lett.* **2016**, *16*, 3179.
- [11] Z. Wu, J. Chen, Y. Mi, X. Sui, S. Zhang, W. Du, R. Wang, J. Shi, X. Wu, X. Qiu, Z. Qin, Q. Zhang, X. Liu, *Adv. Opt. Mater.* **2018**, *6*, 1800674.
- [12] Z. Huang, J. Chen, H. Li, Y. Zhu, Q. Cui, C. Xu, T.-C. Lu, *Adv. Opt. Mater.* **2022**, *10*, 2200603.
- [13] S. Yang, W. Bao, X. Liu, J. Kim, R. Zhao, R. Ma, Y. Wang, X. Zhang, *Matter* **2022**, *4*, 4042.
- [14] L. Zhu, Q. Lai, W. Zhai, B. Chen, Z. Wang, *Mater. Today* **2020**, *37*, 56.
- [15] Z. Yang, M. Jiang, L. Guo, G. Hu, Y. Gu, J. Xi, Z. Huo, F. Li, S. Wang, C. Pan, *Nano Energy* **2021**, *85*, 105951.
- [16] Q. Dong, J. Song, Y. Fang, Y. Shao, S. Ducharme, J. Huang, *Adv. Mater.* **2016**, *28*, 2816.
- [17] J. Sun, Q. Hua, R. Zhou, D. Li, W. Guo, X. Li, G. Hu, C. Shan, Q. Meng, L. Dong, C. Pan, Z. Wang, *ACS Nano* **2019**, *13*, 4507.
- [18] L. Zhu, Z. Wang, *Adv. Funct. Mater.* **2019**, *29*, 1808214.
- [19] C. Pan, L. Dong, G. Zhu, S. Niu, R. Yu, Q. Yang, Y. Liu, Z. Zhong, *Nat. Photonics* **2013**, *7*, 752.
- [20] Q. Yang, Y. Liu, C. Pan, J. Chen, X. Wen, Z. Wang, *Nano Lett.* **2013**, *13*, 607.
- [21] X. Yang, L. Dong, C. Shan, J. Sun, N. Zhang, S. Wang, M. Jiang, B. Li, X. Xie, D. Shen, *Adv. Mater.* **2017**, *29*, 1602832.
- [22] W. Wu, Z. Wang, *Nat. Rev. Mater.* **2016**, *1*, 16031.
- [23] R. Ding, X. Zhang, X. Sun, *Adv. Funct. Mater.* **2017**, *27*, 1702207.
- [24] D. Kim, K. Jo, S. Park, Y. Cho, *Adv. Energy Mater.* **2022**, *12*, 2103329.
- [25] Y. Jiao, S. Yi, H. Wang, B. Li, W. Hao, L. Pan, Y. Shi, X. Li, P. Liu, H. Zhang, C. Gao, J. Zhao, J. Lu, *Adv. Funct. Mater.* **2020**, *31*, 2006243.
- [26] Z. Yang, J. Lu, M. ZhuGe, Y. Cheng, J. Hu, F. Li, S. Qiao, Y. Zhang, G. Hu, Q. Yang, D. Peng, K. Liu, C. Pan, *Adv. Mater.* **2019**, *31*, 1900647.
- [27] J. Lu, Z. Yang, F. Li, M. Jiang, Y. Zhang, J. Sun, G. Hu, Q. Xu, C. Xu, C. Pan, Z. Wang, *Mater. Today* **2019**, *24*, 33.
- [28] J. Lu, C. Xu, F. Li, Z. Yang, Y. Peng, X. Li, M. Que, C. Pan, Z. Wang, *ACS Nano* **2018**, *12*, 11899.
- [29] J. Lu, F. Li, W. Ma, J. Hu, Y. Peng, Z. Yang, Q. Chen, C. Xu, C. Pan, Z. Wang, *Adv. Sci.* **2019**, *6*, 1900916.
- [30] W. Ma, J. Lu, Z. Yang, D. Peng, F. Li, Y. Peng, Q. Chen, J. Sun, J. Xi, C. Pan, *ACS Nano* **2019**, *13*, 5049.
- [31] Y. Peng, J. Lu, D. Peng, W. Ma, F. Li, Q. Chen, X. Wang, J. Sun, H. Liu, C. Pan, *Adv. Funct. Mater.* **2019**, *29*, 1905051.
- [32] A. Ummadisingu, L. Steier, J.-Y. Seo, T. Matsui, A. Abate, W. Tress, M. Grätzel, *Nature* **2017**, *545*, 208.
- [33] Y. Song, W. Liu, Y. Qin, X. Han, W. Li, X. Li, H. Long, D. Li, K. Wang, B. Wang, P. Lu, *Adv. Opt. Mater.* **2020**, *8*, 1901695.
- [34] K. Ren, J. Wang, S. Chen, Q. Yang, J. Tian, H. Yu, M. Sun, X. Zhu, S. Yue, Y. Sun, K. Liu, M. Azam, Z. Wang, P. Jin, S. Qu, Z. Wang, *Laser Photonics Rev.* **2019**, *13*, 1800306.
- [35] S. Liu, S. Sun, C. Gan, A. Águila, Y. Fang, J. Xing, T. Do, T. White, H. Li, W. Huang, Q. Xiong, *Sci. Adv.* **2019**, *5*, eaav9445.
- [36] Q. Zhang, G. Li, X. Liu, F. Qian, Y. Li, T. C. Sum, C. Lieber, Q. Xiong, *Nat. Commun.* **2014**, *5*, 4953.
- [37] C. Huang, W. Sun, Y. Fan, W. W. , Y. Gao, N. Z. , K. Wang, S. Liu, S. Wang, S. Xiao, Q. Song, *ACS Nano* **2018**, *12*, 3865.
- [38] S. Sun, C. Zhang, K. Wang, S. Wang, S. Xiao, Q. Song, *ACS Photonics* **2017**, *4*, 649.
- [39] T. Kao, K.-B. Hong, Y.-H. Chou, J.-F. Huang, F.-C. Chen, T.-C. Lu, *Opt. Express* **2016**, *24*, 20696.
- [40] Y.-H. Hsieh, B.-W. Hsu, K. Peng, K.-W. Lee, C. Chu, S. Chang, H. Lin, T.-J. Yen, Y.-J. Lu, *ACS Nano* **2020**, *14*, 11670.
- [41] Y.-J. Lu, T. Shen, K. Peng, P. Cheng, S. Chang, M.-Y. Lu, C. Chu, T.-F. Guo, H. Atwater, *ACS Photonics* **2021**, *8*, 335.
- [42] D. Xing, C.-C. Lin, P. Won, R. Xiang, T.-P. Chen, A. Kamal, Y.-C. Lee, Y.-L. Ho, S. Maruyama, S. Ko, C. Chen, J.-J. Delaunay, *Adv. Funct. Mater.* **2021**, *31*, 2102375.
- [43] H. Yu, K. Ren, Q. Wu, J. Wang, J. Lin, Z. Wang, J. Xu, R. Oulton, S. Qu, P. Jin, *Nanoscale* **2016**, *8*, 19536.
- [44] H. Li, J.-H. Li, K.-B. Hong, M. Yu, Y.-C. Chung, C.-Y. Hsu, J.-H. Yang, C.-W. Cheng, Z.-T. Huang, K.-P. Chen, T.-R. Lin, S. Gwo, T.-C. Lu, *Nano Lett.* **2019**, *19*, 5017.

- [45] Q. Shang, M. Li, L. Zhao, D. Chen, S. Zhang, S. Chen, P. Gao, C. Shen, J. Xing, G. Xing, B. Shen, X. Liu, Q. Zhang, *Nano Lett.* **2020**, *20*, 6636.
- [46] S. Desai, G. Seol, J. Kang, H. Fang, C. Battaglia, R. Kapadia, J. Ager, J. Guo, A. Javey, *Nano Lett.* **2014**, *14*, 4592.
- [47] L. Qiao, W. Fang, R. Long, O. Prezhdo, *J. Am. Chem. Soc.* **2021**, *143*, 9982.
- [48] S. Guo, Y. Zhao, K. Bu, Y. Fu, H. Luo, M. Chen, M. Hautzinger, Y. Wang, S. Jin, W. Yang, X. Lü, *Angew. Chem., Int. Ed.* **2020**, *59*, 17533.
- [49] Y. Shi, W. Zhao, Z. Ma, G. Xiao, B. Zou, *Chem. Sci.* **2021**, *12*, 14711.
- [50] L. Du, C. Wang, W. Xiong, S. Zhang, C. Xia, Z. Wei, J. Li, S. Tongay, F. Yang, X. Zhang, X. Liu, Q. Liu, *2D Mater.* **2019**, *6*, 025014.
- [51] H. Dong, C. Zhang, X. Liu, J. Yao, Y. Zhao, *Chem. Soc. Rev.* **2020**, *49*, 951.
- [52] A. Glazer, *Acta Cryst.* **1972**, *28*, 3384.
- [53] A. Khan, G. Huang, M. Rana, N. Mei, M. Biondi, S. Rassel, N. Tanguy, B. Sun, Z. Leonenko, N. Yan, C. Wang, S. Xu, D. Ban, *Nano Energy* **2021**, *86*, 106039.
- [54] H. Chen, J. Hu, S. Wang, B. Li, X. Wang, Y. Wang, L. Dai, R. Ma, *Sci. Adv.* **2017**, *3*, e1601962.